Regional scale analysis of climate extremes in an SRM geoengineering simulation, Part 2: temperature extremes

Rohi Muthyala[1,2], Govindasamy Bala[1,]* and Aditya Nalam[1]

[1]Centre for Atmospheric and Oceanic Sciences, Indian Institute of Science, Bengaluru 560 012, India
[2]Present address: Department of Geography, Rutgers, The State University of New Jersey, Piscataway, NJ 08854, USA

In this study, we examine the statistics of temperature extremes in a model simulation of solar radiation management (SRM) geoengineering. We consider both intensity and frequency-based extreme indices for temperature. The analysis is performed over both large-scale domains as well as regional scales (22 Giorgi land regions). We find that temperature extremes are substantially reduced in geoengineering simulation: the magnitude of change is much smaller than that occur in a simulation with elevated atmospheric CO_2 alone. Large increase (~10–20 K) in the lower tails (0.1 percentile) of T_{min} and T_{max} in the northern hemisphere extra-tropics that are simulated under doubling of CO_2 are reduced in geoengineering simulation, but significant increase (~4–7 K) persist over high-latitude land regions. Frequency of temperature extremes is largely offset over land regions in geoengineered climate. We infer that SRM schemes are likely to reduce temperature extremes and the associated impacts on a global scale. However, we note that a comprehensive assessment of moral, social, ethical, legal, technological, economic, political and governance issues is required for using SRM methods to counter the impacts of climate change.

Keywords: Extreme events, geoengineering, regional analysis, solar radiation constant.

INCREASED greenhouse gas (GHG) emissions induce a warmer climate across the globe. This warming is associated with changes in several temperature extreme indices that have been observed and are expected to continue in the future. Several previous studies have shown that solar radiation management (SRM) geoengineering can offset the global mean surface warming caused by increase in GHGs[1–10]. This article is Part 2 of our two-part study on climate extremes under geoengineering. Part 1 discussed changes in precipitation extremes[11] and this Part 2 discusses changes in temperature extremes.

The trend of changes in temperature extremes is similar to that of temperature means in many parts of the world[12]. Changes in indices based on daily minimum temperature are found to be more pronounced than changes in indices based on daily maximum temperature[13]. The shifts toward warmer temperatures of cold extremes are generally larger than the corresponding shifts of warm extremes in high-latitude regions[12]. In tropical and subtropical regions, warm extremes shift toward warmer temperatures faster than cold extremes.

Only a few studies in the past have investigated the statistics of temperature extremes under SRM geoengineering. Using daily model output the frequency of temperature extreme events such as coldest night, warmest day and a few duration indices was analysed[14]. The study showed that the climate extremes under geoengineering are not just smaller than 4XCO2 conditions, but they also differ significantly from those under pre-industrial conditions. It was also found that geoengineering is more effective in reducing changes in temperature extremes compared to precipitation extremes and more effective in reducing changes in precipitation extremes than means, but less effective in reducing changes in temperature extremes compared to means[14]. Another study analysed climate extremes for two SRM schemes[15] – stratospheric sulphate injection and marine cloud brightening. In both climate engineering scenarios, extreme temperature changes were similar to mean temperature changes over much of the globe, except over the northern hemisphere high latitudes. The increase in frequency of temperature extremes was not completely alleviated in both geoengineering scenarios.

In this article, we perform an extensive assessment of the temperature extremes using 16 indices (12 for intensity and 4 for frequency) and their projected changes in geoengineered climate. We analyse a few percentile indices (upper and lower tails) to account for the respective climatologies of different regions. Further, we quantify the changes in extremes over 22 Giorgi land regions and several large domains.

Model, experiments and methodology

As discussed in Part 1, the model used for this study is the National Center for Atmospheric Research (NCAR)

Table 1. Set of temperature extreme indices analysed in this study. These indices are recommended by the Expert Team of Climate Change Detection and Indices, except those marked with an asterisk

Label	Index	Index definition	Units
TNn	Coldest daily T_{min}	Annual minimum value of daily minimum temperature TN	K
TNx	Warmest daily T_{min}	Annual maximum value of daily minimum temperature TN	K
TXn	Coldest daily T_{max}	Annual minimum value of daily maximum temperature TX	K
TXx	Warmest daily T_{max}	Annual maximum value of daily maximum temperature TX	K
0.1TN*	Lower extreme T_{min}	Intensity of daily minimum temperature events which do not exceed 0.1th percentile threshold	K
99.9TN*	Upper extreme T_{min}	Intensity of daily minimum temperature events which exceed 99.9th percentile threshold	K
0.1TX*	Lower extreme T_{max}	Intensity of daily maximum temperature events which do not exceed 0.1th percentile threshold	K
99.9TX*	Upper extreme T_{max}	Intensity of daily maximum temperature events which exceed 99.9th percentile threshold	K
TN10p	Cold nights	Let TN_{th} 10 be the 10th percentile of TN in 1XCO2 simulation. The percentage of days in a year with $TN < TN_{th} 10$	%
TN90p	Warm nights	Let TN_{th} 90 be the 90th percentile of TN in 1XCO2 simulation. The percentage of days in a year with $TN > TN_{th} 90$	%
TX10p	Cold days	Let $TX_{th}10$ be the 10th percentile of TX in 1XCO2 simulation. The percentage of days in a year with $TX < TX_{th} 10$	%
TX90p	Warm days	Let TX_{th} 90 be the 90th percentile of TX in 1XCO2 simulation. The percentage of days in a year with $TX > TX_{th} 90$	%
FD	Frost days	Number of days when $TN < 0°C$	days
ID	Ice days	Number of days when $TX < 0°C$	days
SU	Summer days	Number of days when $TX > 25°C$	days
TR	Tropical nights	Number of days when $TN > 20°C$	days

Community Earth System Model, version 1 (CESM1)[16]. Three experiments have been performed: (i) a pre-industrial control simulation '1XCO2', (ii) '2XCO2' with doubled atmospheric CO_2 concentration and (iii) 'Geo-Engg' with doubled atmospheric CO_2 concentration and the solar constant reduced. A detailed explanation of the model used and the experiments performed are provided in Part 1 of this study[11].

The model-simulated temperature indices were evaluated using the daily data from the National Center for Environmental Prediction–Department of Energy (NCEP–DOE) Reanalysis 2 (http://www.esrl.noaa.gov/psd/). This is an improved version of NCEP 1 that fixed errors and updated parameterization of physical processes. State-of-the-art analysis/forecast system was used to perform data assimilation with past data from 1979. The horizontal resolution of the data was $2.0° \times 2.0°$.

Here, we consider a subset of temperature extreme indices available in EIA (ETCCDI Indices Archive). We quantify the temperature extreme events in terms of both intensity and frequency. The control simulation (1XCO2) thresholds are used as reference thresholds in estimating indices instead of a base observational threshold. Four new temperature indices – 0.1TN, 99.9TN, 0.1TX and 99.9TX – have been added to our set of extreme temperature indices. The first index, i.e. 0.1TN represents the 0.1th percentile threshold value of daily minimum temperature; 99.9TN is the intensity of daily minimum temperature events which exceed 99.9th percentile threshold. Similarly, 0.1TX and 99.9TX are defined for daily maximum temperature. The selected indices (Table 1) give a comprehensive overview of changes in temperature and precipitation extremes in both 2XCO2 and

geoengineering scenarios[13,17]. Regional extreme value statistics was performed for various selected regions (Supplementary Table 1) and for Giorgi land regions (Supplementary Table 2 and Figure 1)[18]. Spatial statistical analysis was also performed to estimate their uncertainties at local scale. Estimates for land and ocean regions were also performed.

Methodology for estimating all temperature extreme indices is not similar. We used three methods of aggregating individual events to create samples. The first method aggregates the events for the whole time period (over the entire 10-year period in this study) for each grid point. Then temperature extremes are estimated at each grid point based on their respective index definition and statistical analysis is performed over the spatial domain of interest. The second method aggregates the individual events on the annual timescale at each grid point to create the sample; then climate extremes are estimated from these samples and the mean of these extremes over the 10-year time period is calculated at each grid point. Then statistical analysis is performed over the selected spatial domains. The second method is suitable for estimating the annual indices (FD, TR, TNn, TXx, etc.), while the first method is suitable for the other indices. The third method, suitable for estimating zonal means of extremes, aggregates individual events over the 10-year period to estimate climate extreme events at each grid point and then averages along each latitude circle.

Results

In this article, we discuss the changes in temperature extremes in a doubled CO_2 (2XCO2) and geoengineered
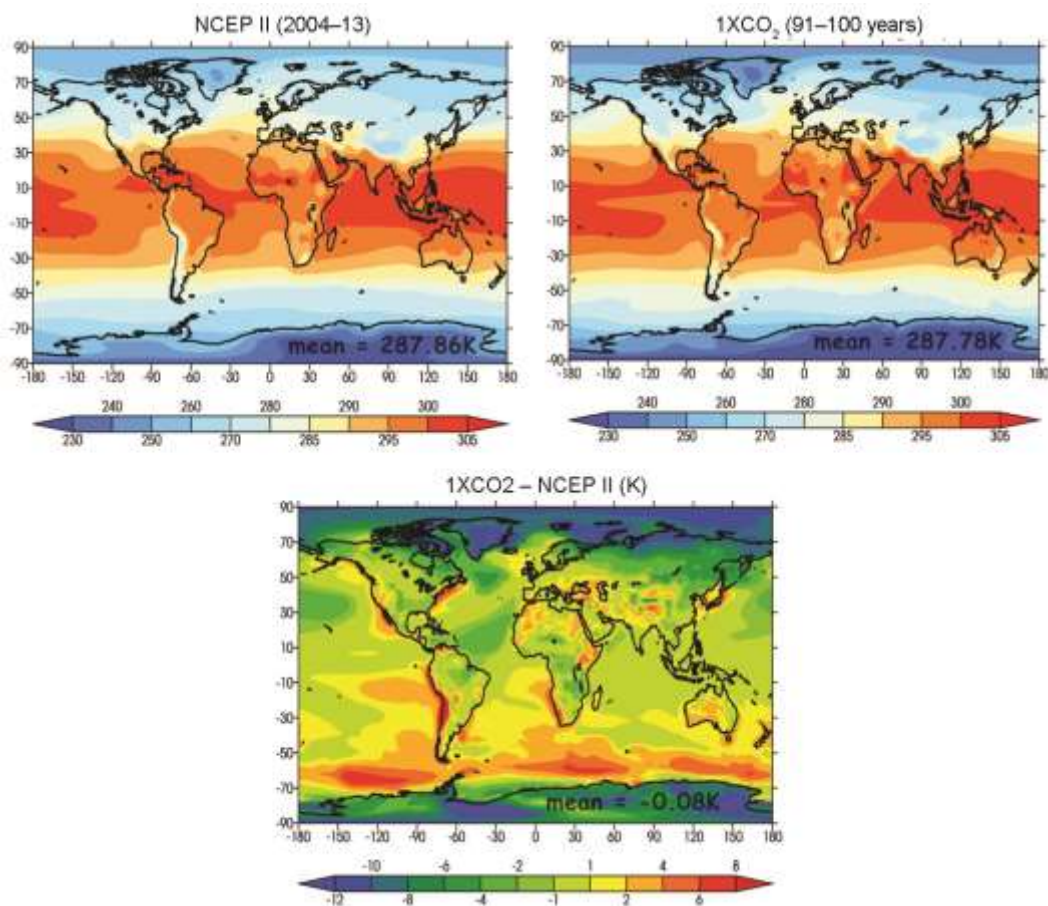
Figure 1. (Top) Spatial pattern of annual mean surface temperature for NCEP II (reanalysis data for 2004–2013; top left panel) and 1XCO2 (control simulation during 91–100 years; top right panel). (Bottom panel) Difference between model simulation and reanalysis data.

climate (Geo-Engg) relative to the 1XCO2 case. The changes in precipitation and temperature means in a geoengineered climate have been discussed in several previous studies[1,2,8–10,19–22]. In the 2XCO2 case, we found that the change in mean surface temperature was 4.1 K and mean precipitation was 0.24 mm/day (7.9%). However, in the Geo-Engg case the change in global mean temperature reduced to –0.07 K and precipitation to –0.08 mm/day (–2.8%).

Evaluation of model-simulated temperature extremes

We found that the model-simulated surface mean temperature showed a spatial pattern similar to that in NCEP II reanalysis data (for the period 2004–2013; correlation coefficient of 0.99) with a global mean difference of –0.08 K (Figure 1). The model underestimated the surface temperature over extra-tropical land regions, but overestimated the same in the ocean areas of the southern hemisphere. Figure 2 shows a comparison of annual maximum and minimum temperature. The pattern is similar for the daily minimum temperature extremes with a cor-

relation coefficient of 0.97 and the mean bias is small (Figure 2). However, daily maximum temperature extremes show similar pattern (correlation coefficient of 0.95) in the 1XCO2 case and reanalysis data with an overestimation over most of the land regions (mean bias = 5.5 K). Hence, the minimum temperature extremes are slightly underestimated and the maximum temperature extremes are overestimated. The extreme temperature frequency indices were also evaluated ([Supplementary Figures 2 and 3](#)). We found that the frequency indices showed similar pattern (correlation coefficient of FD was 0.98, TR was 0.92, SU was 0.95) to reanalysis data. Tropical nights were slightly underestimated ([Supplementary Figure 4)](#) (mean bias ;18 days) and summer days were slightly overestimated over tropical land regions ([Supplementary Figure 3](#)) (mean bias ~32 days). The daily minimum indices were slightly underestimated over high-latitude land regions and daily maximum indices overestimated over mid- and low-latitude land regions (Figure 2), thereby overestimating the diurnal range by a large bias ([Supplementary Figure 3](#)) (mean bias ~8 K) and also with a smaller correlation coefficient of 0.46. Overall, we found the spatial pattern in
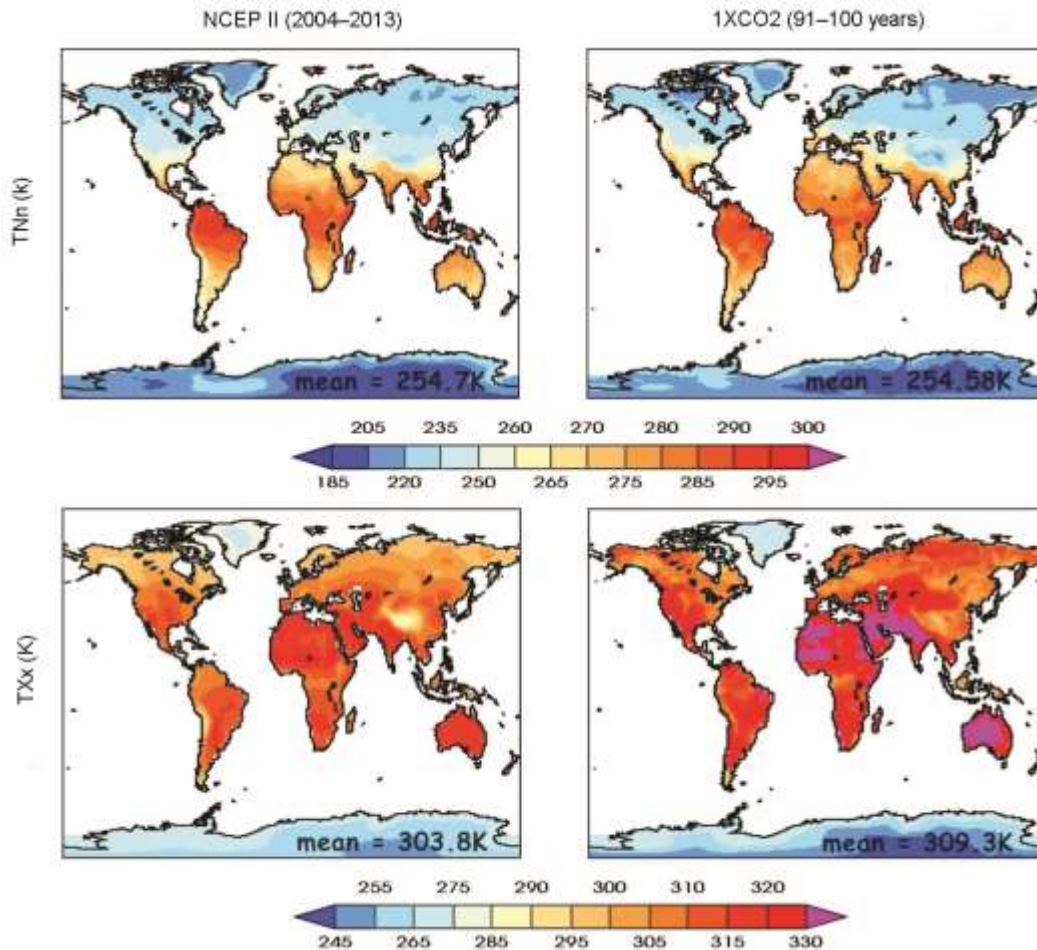
Figure 2. Spatial pattern of TNn (annual minimum daily minimum temperature; top panels) and TXx (annual maximum daily maximum temperature; bottom panels; description of the indices is given in Table 1) for NCEP II (reanalysis data for 2004–13; left panels) and 1XCO2 (control simulation for 91–100 years; right panels).

model-simulated extremes, annual temperature maximum and minimum to be in good agreement with NCEP II reanalysis. However, there were large regional biases in daily maximum temperature extreme indices, but when we compare two model simulations, it is likely that the biases will cancel out.

Changes in intensity of temperature extremes

We analysed the intensity of temperature extremes using the four absolute indices: annual maximum and minimum of T_{max} and T_{min}, i.e. TNn, TNx, TXn and TXx (Table 1). We also used four percentile indices: 0.1TN, 99.9TN, 0.1TX and 99.9TX (Table 1). The probability density function (PDF) of surface temperature and threshold for extreme temperature events would be different at every grid point, and hence these indices were estimated at each grid point. This avoids errors in analysing the extremes due to nonuniformity in temperature ranges on a regional scale.

In the 2XCO2 case, we found a large increase of 10–15 K in daily minimum temperature indices (TNn and TNx) and 4–6 K in daily maximum temperature indices (TXn and TXx) in the high latitudes (Supplementary Figure 4). However, in the Geo-Engg case, this increase was largely offset in daily maximum indices, but residual warming (~5 K) persisted in daily minimum indices over mid- and high-latitude land regions in the northern hemisphere. From the spatial pattern of changes in 0.1TN (lower extreme T_{min}) and 99.9TX (upper extreme T_{max}), we found that in the 2XCO2 case there was global mean increase of 5.1 K in 0.1TN and 3.6 K in 99.9TX (Supplementary Figure 5), while the surface mean temperature increase was 4.1 K (Supplementary Figure 6). We found that there was a large increase of ~20 K in 0.1TN over some extra-tropical oceanic regions and around 10 K in 99.9TX over northern extra-tropical oceanic region (Supplementary Figure 5). In the Geo-Engg case, the temperature extremes were brought close to the 1XCO2 case on a global scale (Figures 3a and 4a). However, on the regional scale, we found that whereas the medians of
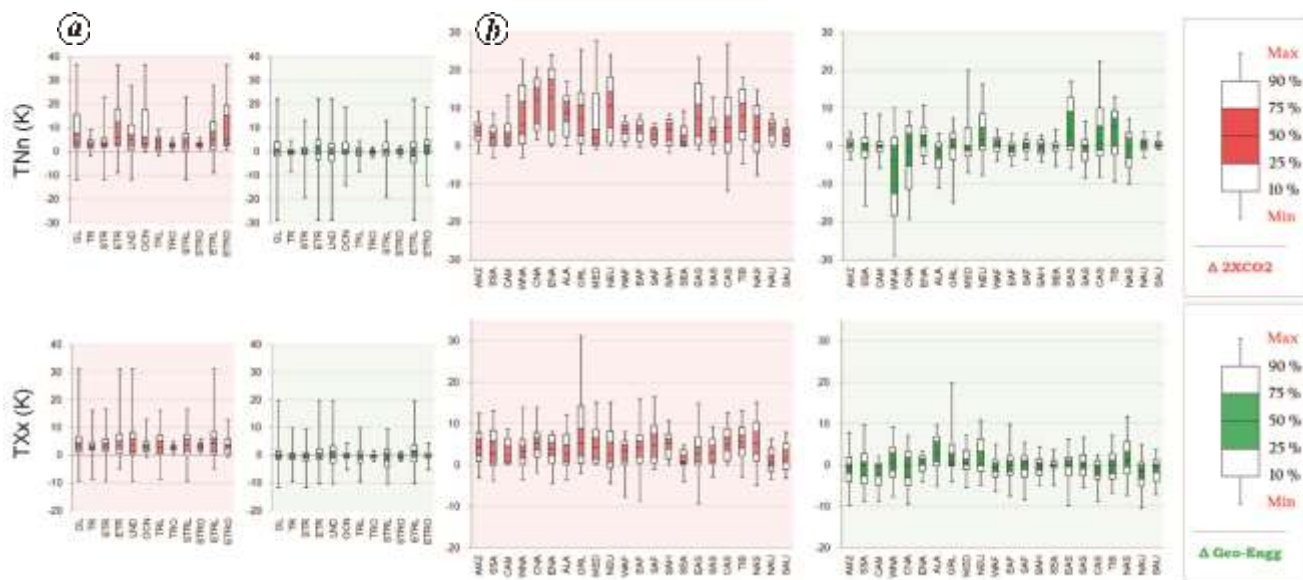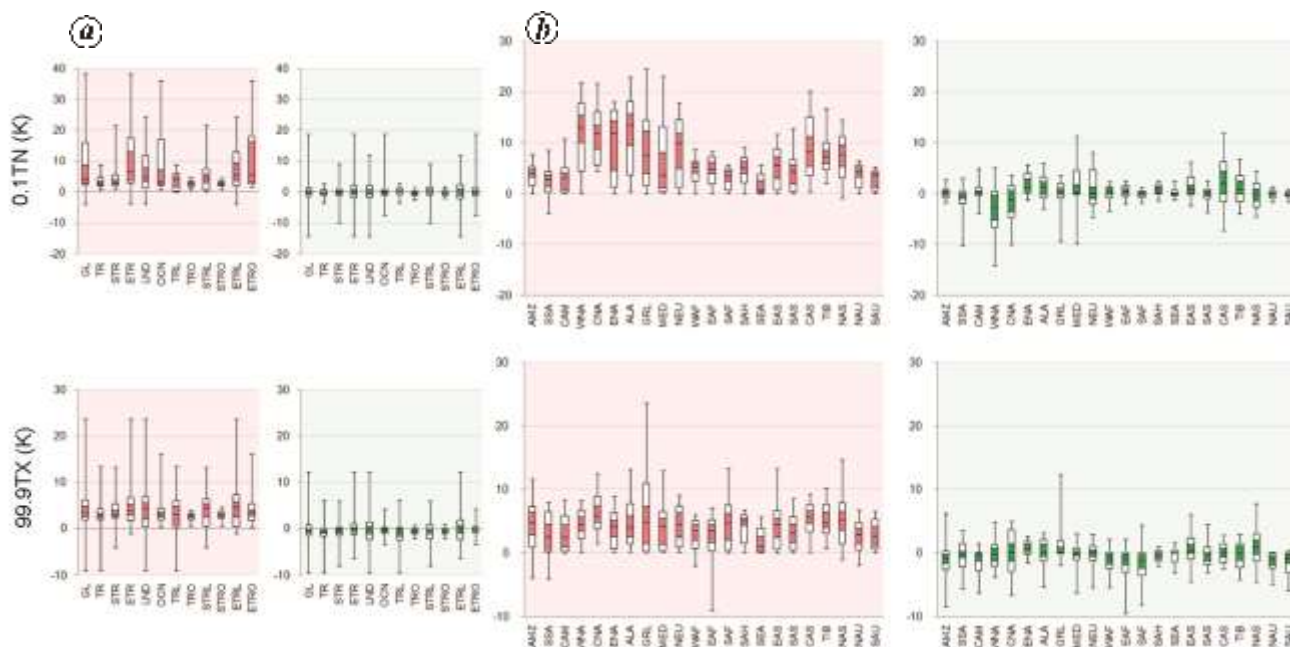
Figure 3. Change in intensity of temperature extremes in the 2XCO2 (red) and Geo-Engg (green) cases relative to the 1XCO2 case, represented using two indices TNn (coldest daily T_{min}; top panels) and TXx (warmest daily T_{max}; bottom panels; descriptions of the indices are given in Table 1) for (**a**) large domains and (**b**) Giorgi land regions.

Figure 4. Change in intensity of temperature extremes in the 2XCO2 (red) and Geo-Engg (green) cases relative to the 1XCO2 case, represented using the two indices 0.1TN (lower extreme T_{min}; top panels) and 99.9TX (upper extreme T_{max}; bottom panels; description of the indices is given in Table 1) for (**a**) large domains and (**b**) Giorgi land regions.

changes were nearly zero in 0.1TN and 99.9TX, extremes still existed over a wide range on a local scale for most of the land regions (Figures 3 *b* and 4*b*).

The changes in other tails of daily minimum and maximum temperature indices (TNx, TXn, 99.9TN and 0.1TX) followed similar pattern when compared to the indices TXx, TNn, 99.9TX and 0.1TN (Supplementary Figures 7 and 8). Both intensity-based indices TNn, TXx and 0.1TN, 99.9TX followed similar pattern, but the magnitude of changes in conventional absolute indices (TNn and TXx) was larger than the percentile indices (0.1TN and 99.9TX) in the Geo-Engg case (compare the right panels of Supplementary Figures 4 and 5). In summary, upper extreme T_{max} in the Geo-Engg case was
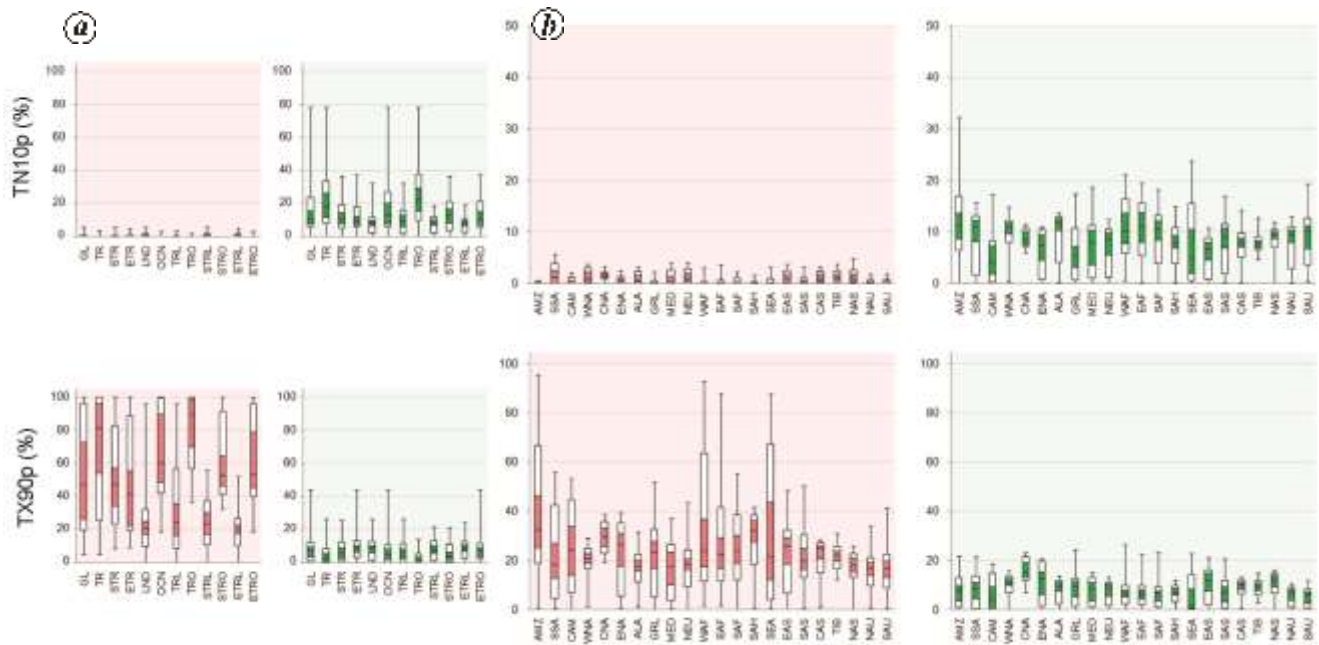
Figure 5. Change in frequency of temperature extremes in the 2XCO2 (red) and Geo-Engg (green) cases relative to the 1XCO2 case, represented using the two indices TN10p (cold nights; top panels) and TX90p (warm days; bottom panels; description of the indices is given in Table 1) for (*a*) large domains and (*b*) Giorgi land regions.

closer to the 1XCO2 case and changes in lower extreme T_{min} remained slightly positive on the regional scale.

Changes in frequency of temperature extremes

We analysed the frequency of temperature extremes using the eight indices: cold nights (TN10p), warm nights (TN90p), cold days (TX10p), warm days (TX90p), frost days (FD), ice days (ID), summer days (SU) and tropical nights (TR) (Table 1). These indices were estimated at each grid point annually and then averaged over the 10-year period (91–100 years). The indices TN10p, TN90p, TX10p and TX90p were estimated for the 2XCO2 and Geo-Engg cases relative to the 1XCO2 case (Supplementary Figure 2). In Figure 5 (see also Supplementary Figures 9 and 10), a value of 10 corresponds to no change in extremes (relative to the 1XCO2 case). In the 2XCO2 case, 10th percentile of minimum and maximum temperature of the 1XCO2 case reduced to about 0.2th percentile on a global mean basis, thereby resulting in decrease in occurrence of cold days and nights (TN10p and TX10p) (Figure 5 *a*; also see Supplementary Figure 9 and 10 *a*). However, in the Geo-Engg case, the cold days (TX10p) and nights (TN10p) increased to ~15% (Supplementary Figure 9). On a regional scale, the frequency of temperature extremes in the Geo-Engg case was nearly similar to that in the 1XCO2 case (Figure 5 *b* and also see Supplementary Figure 10 *b*). Similarly, in the

2XCO2 case, the occurrence of warm days and nights (TN90p and TX90p) increased to ~60% from 10% in the 1XCO2 case. However, in the Geo-Engg case, we found that the frequency of temperature extremes was close to the 1XCO2 case over land regions. Over the ocean areas, the lower extreme indices (TN10p and TX10p) were slightly larger than those in the 1XCO2 case and upper extreme indices (TN90p and TX90p) were slightly less than those in the 1XCO2 case. Overall, there was a shift in the PDF of temperature to the left: SRM geoengineering slightly reduced the warm temperature extremes and increased the cold extremes relative to the 1XCO2 case. For example, TN90p decreased to 5.5% and TN10p increased to 14.7%, indicating that the number of warm nights decreased and that of cold nights increased in the Geo-Engg case.

The spatial pattern of FD and SU showed that the former reduced by 16 days per annum on a global mean basis and the latter increased by 42 days per annum in the 2XCO2 case (Supplementary Figure 11). Regionally, there were large differences: large reduction of 150–200 days in the number of frost days was found in the high latitudes and large increase of 200–250 days in the number of summer days was found in subtropical oceanic regions. In contrast, we simulated large reduction in the frequency of temperature extremes in the Geo-Engg case when compared to the 2XCO2 case, which were brought close to the 1XCO2 case globally (Supplementary Figure 11). Over large domains, the changes in medians of both FD and SU were close to zero in the Geo-Engg case (Figure 6 *a*). On the regional scale, we found that in the
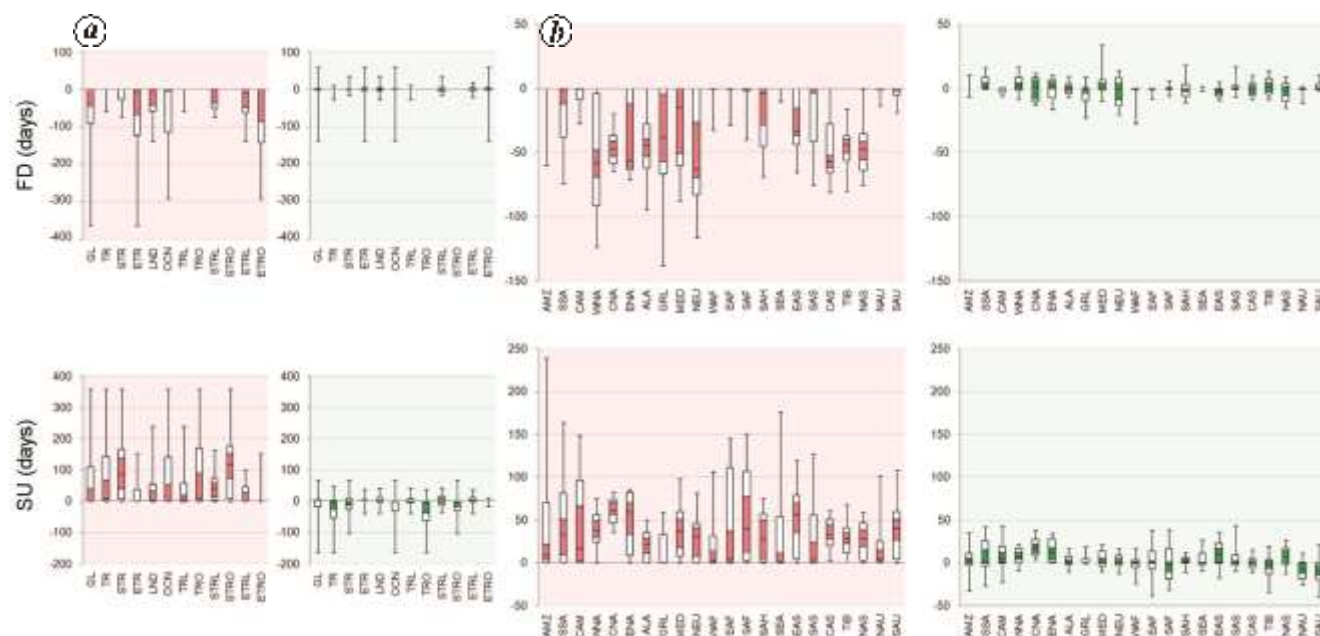
Figure 6. Change in frequency of temperature extremes in the 2XCO2 (red) and Geo-Engg (green) cases relative to the 1XCO2 case, represented using the two indices FD (frost days; top panels) and SU (summer days; bottom panels; description of the indices is given in Table 1) for (**a**) large domains and (**b**) Giorgi land regions.

Geo-Engg case the frequency of temperature extremes (FD and SU) reduced to a large extent when compared to the 2XCO2 case (Figure 6 *b*). The changes in medians were close to zero and simultaneously the spatial variability (length of whiskers) is also reduced to a large extent. The changes in ID and TR followed patterns similar to those FD and SU (Supplementary Figures 11 and 12).

Changes in zonal mean intensity and frequency of temperature extremes

The zonal mean intensity of temperature extremes (0.1TN and 99.9TX) showed that in the 2XCO2 case the zonal mean intensity of temperature extremes was 3–5 K larger than those in the 1XCO2 case (Figure 7 *a* and *b*). However, the zonal mean of frequency of FD was 10–20 days and 40–50 days less than that in the 1XCO2 case over the southern hemisphere high latitudes and northern hemisphere mid- and high-latitudes respectively (Figure 7 *c*). We also found that the zonal mean frequency of SU was 50–100 days larger than that in the 1XCO2 case over the tropics and subtropics (Figure 7 *d*). In contrast, geoengineered climate showed zonal mean of both intensity and frequency of temperature extremes (0.1TN, 99.9TX, FD and SU) similar to that in the 1XCO2 case, except SU over the southern tropics where we found a slight reduction. Overall, we found that the zonal mean temperature extremes were brought closer to pre-industrial climatic conditions by geoengineering. Absolute temperature indices (TNn and TXx) also showed

similar results to 0.1TN and 99.9TX in all the simulations (Supplementary Figure 13).

Comparison of changes in temperature means and extremes

We used changes in 99.9TX (daily maximum extreme) and 0.1TN (daily minimum extreme) to represent the temperature extremes for comparison with surface mean temperature changes (Figure 8). In the 2XCO2 case, we found that the global changes in 0.1TN were larger than those in the mean, whereas changes in 99.9TX were smaller than those in the mean relative to the 1XCO2 case. For other regions (tropics and subtropics), the changes in the means and extremes did not differ significantly. The range of changes in means was around 2.5–5.5 K whereas it was 2.5–8 K for the changes in daily minimum extreme 0.1TN (Figure 8 *a*), with the largest increase simulated for the extra-tropics. On a regional scale (Figure 8 *b*), the range increased to 2–13 K. Our results are qualitatively consistent with previous studies[13]. However, in the Geo-Engg case the extreme temperatures were not only offset but were slightly less than in the 1XCO2 case. We found a reduction of 0.5–1 K in daily maximum extreme over the tropics and subtropics with a maximum reduction of 1 K over tropical land region (Figure 8 *a*). Overall, we found that though there were regional disparities in the geoengineering simulations, temperature means and extremes were close to the 1XCO2 case. Absolute temperature indices (TNn and
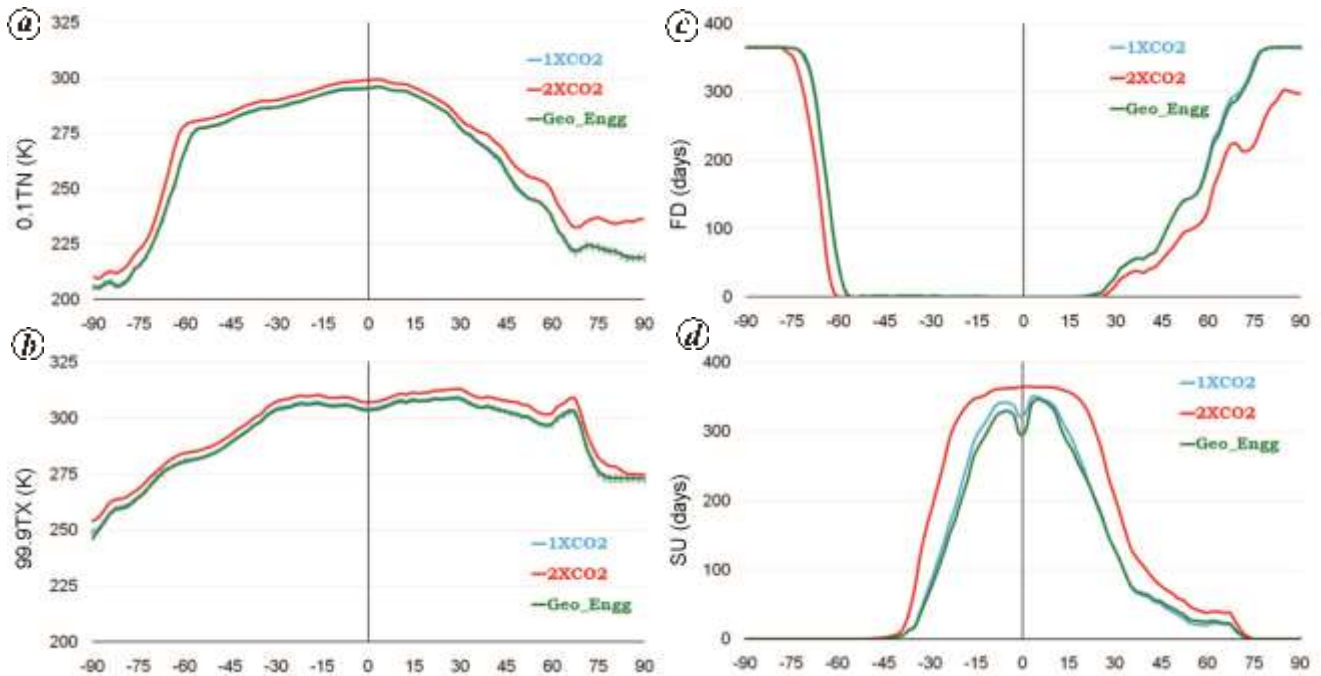
Figure 7. Zonal mean of (*a*, *b*) intensity of extreme temperature (0.1TN and 99.9TX) and (*c*, *d*) frequency of extreme temperature (FD and SU) for 10-year analysis period (91–100 years period in our simulations) calculated for the control (1XCO2; blue), doubled CO_2 (2XCO2; red) and geoengineering (Geo-Engg; green) simulations. Grey bars represent the range of extremes in ten 5-years segments of the last 50-years data of the control simulation (1XCO2).

TXx) also showed similar results to 0.1TN and 99.9TX in all the simulations (Supplementary Figure 14).

Discussion and conclusion

Similar to Part 1 where the precipitation extremes were studied, here we have analysed the temperature extremes in a doubled CO_2 climate with and without geoengineering and compared them with a control simulation using a subset of temperature indices available in EIA and some new temperature indices appropriately defined for this study (Table 1). We have analysed four intensity-based and eight frequency-based temperature extreme indices, and discuss the changes in these indices upon CO_2 doubling and SRM geoengineering.

In the 2XCO2 case, we simulated an increase in global mean temperature of ~4.1 K, daily minimum temperature (0.1TN) of ~5.1 K and daily maximum temperature (99.9TX) of ~3.6 K relative to the 1XCO2 case. However, on a regional scale we simulated large changes in temperature extremes of up to ~20 K mainly in the extra-tropical regions. Temperature extremes were reduced considerably in the Geo-Engg case compared to the 2XCO2 case, with departures from the 1XCO2 case smaller than those in the 2XCO2 case. Though the temperature extremes in the Geo-Engg case were brought close to those in the 1XCO2 case, they were not uniformly reduced over the globe. The change in intensity of

temperature extremes persisted over high latitudes in the northern hemisphere. On a regional scale, upper extremes were brought close to the 1XCO2 case, while the residual changes in lower extremes remained.

The frequency of cold nights (TN10p) and cold days (TX10p) decreased, whereas that of warm nights (TN90p) and warm days (TN90p) increased by up to ~50% in the 2XCO2 case relative to the 1XCO2 case. Similarly, in the 2XCO2 case, we simulated a reduction in the number of frost days (16 days per year decrease) and increase in the number of summer days (42 days per year increase) relative to the 1XCO2 case. In the Geo-Engg case, there was a leftward shift in the PDF of temperature resulting in a small reduction in the warm temperature extremes (TN90p) and increase in the cold temperature extremes (TN10p) relative to the 1XCO2 case. We found that changes in FD and SU in the 2XCO2 case relative to the 1XCO2 case were offset in the Geo-Engg case to a large extent. We also simulated a reduction in the medians in the Geo-Engg case when compared to the 1XCO2 case.

As discussed in Part I, there are several limitations to this study, as we use idealized experiments to demonstrate the effects of SRM geoengineering on climate extremes. Some of the limitations are related to the use of a single model and absence of feedbacks on longer time-scales (deep ocean and carbon cycle feedbacks), as we have used a slab ocean model. We simulated temperature extremes that were close to the observations, but with some biases on a regional scale. Although we used a
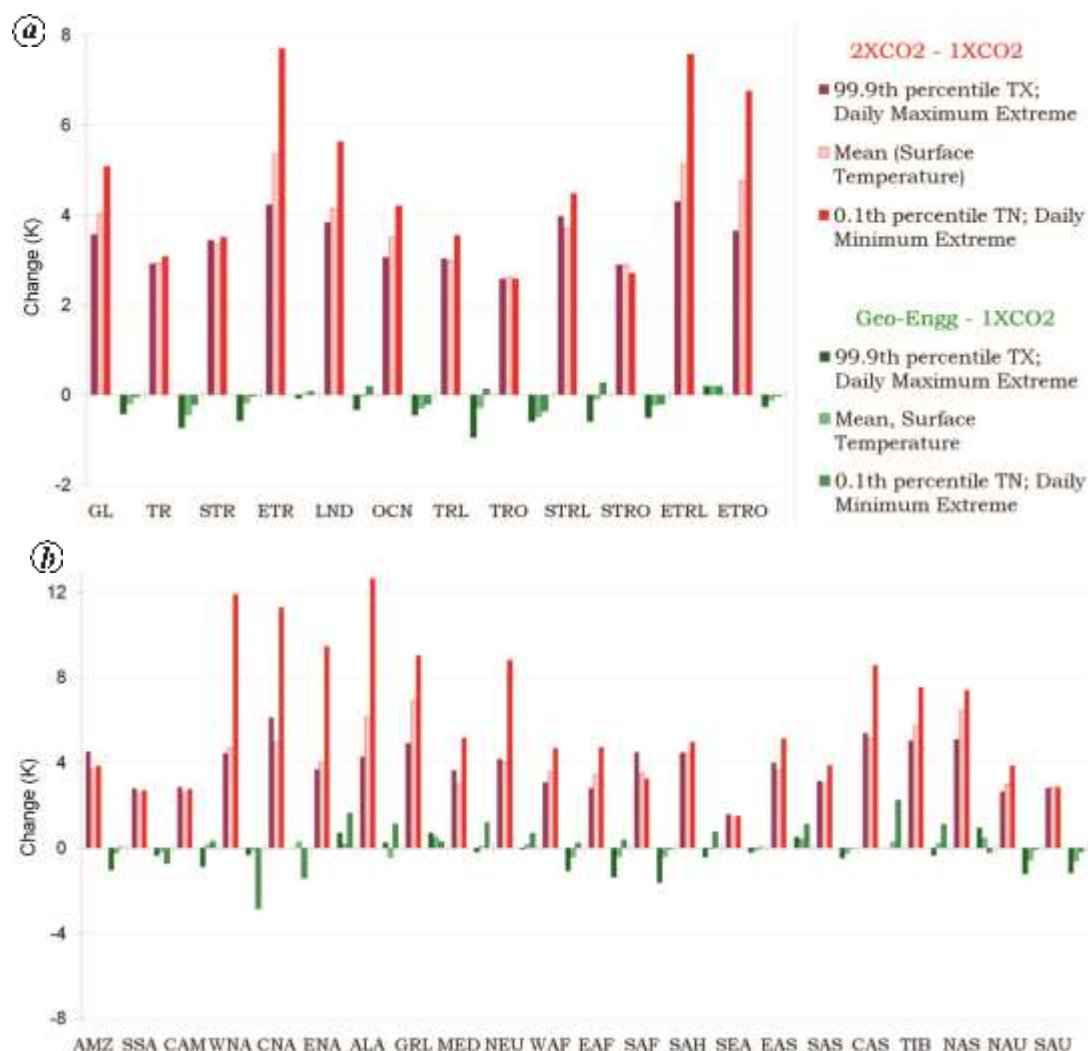
Figure 8. Change in temperature means and extremes (99.9TX and 0.1TN) over (*a*) large domains and (*b*) 22 Giorgi land regions in the 2XCO2 (red bars) and Geo-Engg cases (green bar) relative to the 1XCO2 case.

single model with some limitations, our results are qualitatively in agreement with previous SRM geoengineering studies using solar constant reduction that analysed climate extremes from multiple models[10,14].

In conclusion, we find that geoengineering has the potential to ameliorate the impacts of climate change from extreme events. However, there could be undesired side effects such as ozone depletion for stratospheric aerosol injections[6] and several reasons for not considering geoengineering to counter climate change[23]. Also, a comprehensive assessment of the moral, social, ethical, legal, technological, economic, political and governance issues related to geoengineering needs to performed before implementation of any SRM geoengineering methods. In the absence of a global consensus on these issues, reducing GHG emissions is likely the best strategy to tackle climate change.

1. Govindasamy, B. and Caldeira, K., Geoengineering earth's radiation balance to mitigate CO_2-induced climate change. *Geophys. Res. Lett.*, 2000, **27**, 2141–2144; doi:10.1029/1999GL006086.
2. Govindasamy, B., Thompson, S., Duffy, P. B., Caldeira, K. and Delire, C., Impact of geoengineering schemes on the terrestrial biosphere. *Geophys. Res. Lett.*, 2002, **29**(22), 2061; doi:10.1029/2002GL015911.
3. Govindasamy, B., Caldeira, K. and Duffy, P. B., Geoengineering earth's radiation balance to mitigate climate change from a quadrupling of CO_2. *Global Planet Change*, 2003, **37**(1–2), 157–168; doi:10.1016/S0921-8181(02)00195-9.
4. Matthews, H. D. and Caldeira, K., Transient climate–carbon simulations of planetary geoengineering. *Proc. Natl. Acad. Sci. USA*, 2007, **104**, 9949–9954; doi:10.1073/pnas.0700419104.
5. Robock, A., Oman, L. and Stenchikov, G. L., Regional climate responses to geoengineering with tropical and Arctic SO_2 injections. *J. Geophys. Res.*, 2008, **113**, D16101; doi:10.1029/2008JD010050.
6. Rasch, P. J. *et al.*, An overview of geoengineering of climate using stratospheric sulphate aerosols. *Philos. Trans. R. Soc. London, Ser. A*, 2008, **366**, 4007–4037; doi:10.1098/rsta.2008.013.
7. Ricke, K. L., Granger Morgan, M. and Allen, M. R., Regional climate response to solar-radiation management. *Nature Geosci.*, 2010, **3**, 537–541; doi:10.1038/ngeo915.

8. Schmidt, H. *et al.*, Solar irradiance reduction to counteract radiative forcing from a quadrupling of CO_2: climate responses simulated by four earth system models. *Earth Syst. Dyn.*, 2012, **3**, 63–78; doi:10.5194/esd-3-63-2012.

9. Kravitz, B. *et al.*, Climate model response from the Geoengineering Model Intercomparison Project (GeoMIP). *J. Geophys. Res. Atmos.*, 2013, **118**, 8320–8331; doi:10.1002/jgrd.50646.

10. Tilmes, S. *et al.*, The hydrologic impact of Geoengineering in the Geoengineering Model Intercomparison Project (GeoMIP). *J. Geophys. Res. Atmos.*, 2013, **118**(11036–11), 058; doi:10.1002/jgrd.50868.

11. Muthyala, R., M., Bala, G. and Nalam, A., Regional scale analysis of climate extremes in an SRM geoengineering simulation, Part 1: precipitation extremes. *Curr. Sci.*, 2018, **114**(5), 1024–1035.

12. Kharin, V. V., Zwiers. F. W., Zhang, X. and Hegerl, G. C., Changes in temperature and precipitation extremes in the IPCC ensemble of global coupled model simulations. *J. Climate*, 2007, **20**, 1419–1444; doi:10.1175/JCLI4066.1.

13. Sillmann, J., Kharin, V. V., Zhang, X., Zwiers, F. W. and Bronaugh, D., Climate extreme indices in the CMIP5 multi-model ensemble: Part 2. Future climate projections. *J. Geophys. Res. Atmos.*, 2013, **118**, 2473–2493; doi:10.1002/jgrd.50188.

14. Curry, C. L. *et al.*, A multimodel examination of climate extremes in an idealized geoengineering experiment. *J. Geophys. Res. Atmos.*, 2014, **119**, 3900–3923; doi:10.1002/2013JD020648.

15. Aswathy, V. N., Boucher, O., Quaas, M., Niemier, U., Muri, H. and Quaas, J., Climate extremes in multi-model simulations of stratospheric aerosol and marine cloud brightening climate engineering. *Atmos. Chem. Phys. Discuss.*, 2014, **14**, 32393–32425; doi:10.5194/acpd-14-32393-2014.

16. Richard, B. N. *et al.*, Description of the NCAR Community Atmosphere Model (CAM 5.0). NCAR Technical Note NCAR/TN-464 + STR, National Centre for Atmospheric Research, Boulder, CO, USA, 2012.

17. Sillmann, J., Kharin, V. V., Zhang, X., Zwiers, F. W. and Bronaugh, D., Climate extreme indices in the CMIP5 multi-model ensemble: Part 1. Model evaluation in the present climate. *J. Geophys. Res. Atmos.*, 2013, **118**, 1716–1733; doi:10.1002/jgrd.50203.

18. Giorgi, F. and Francisco, R., Uncertainties in regional climate change prediction: a regional analysis of ensemble simulations with the HADCM2 coupled AOGCM. *Climate Dyn.*, 2000, **16**, 169–182.

19. Bala, G., Duffy, P. B. and Taylor, K. E., Impact of geoengineering schemes on the global hydrological cycle. *Proc. Natl. Acad. Sci. USA*, 2008, **105**, 7664–7669; doi:10.1073/pnas.0711648105.

20. Bala, G., Caldeira, K., Nemani, R., Cao, L., Ban-Weiss, G. and Shin, H. J., Albedo enhancement of marine clouds to counteract global warming: impacts on the hydrological cycle. *Climate Dyn.*, 2010, **37**(5–6), 915–931; doi:10.1007/s00382-010-0868-1.

21. Bala, G. and Nag, B., Albedo enhancement over land to counteract global warming: impacts on hydrological cycle. *Climate Dyn.*, 2012, **39**, 1527–1542; doi:10.1007/s00382-011-1256-1.

22. Kalidindi, S., Bala, G., Modak, A. and Caldeira, K., Modeling of solar radiation management: a comparison of simulations using reduced solar constant and stratospheric sulphate aerosols. *Climate Dyn.*, 2015, **44**, 2909–2925; doi:10.1007/s00382-014-2240-3.

23. Robock, A., 20 Reasons why geoengineering may be a bad idea. *Bull. Atmos. Sci.*, 2008, **64**(2), 14–18, 59; doi:10.2968/064002006.